Diffusion-Weighted Magnetic Resonance Imaging for Predicting and Detecting Early Response to Chemoradiation Therapy of Squamous Cell Carcinomas of the Head and Neck

Sungheon Kim,[1] Laurie Loevner,[1] Harry Quon,[2] Eric Sherman,[3] Gregory Weinstein,[4] Alex Kilger,[1] and Harish Poptani[1]

Abstract

Purpose: The aim of this study was to investigate the utility of apparent diffusion coefficient (ADC) for prediction and early detection of treatment response in head and neck squamous cell carcinomas (HNSCC).

Experimental Design: Diffusion-weighted magnetic resonance imaging studies were performed on 40 patients with newly diagnosed HNSCC before, during, and after the end of chemoradiation therapy. Analysis was done on data from 33 patients after exclusion of 7 patients that had incomplete data.

Results: Pretreatment ADC value of complete responders ($1.04 \pm 0.19 \times 10^{-3}$ mm^2/s) was significantly lower ($P < 0.05$) than that from partial responders ($1.35 \pm 0.30 \times 10^{-3}$ mm^2/s). A significant increase in ADC was observed in complete responders within 1 week of treatment ($P < 0.01$), which remained high until the end of the treatment. The complete responders also showed significantly higher increase in ADC than the partial responders by the first week of chemoradiation ($P < 0.01$). When pretreatment ADC value was used for predicting treatment response, the area under the receiver operating characteristic curve was 0.80 with a sensitivity of 65% and a specificity of 86%. However, change in ADC within the first week of chemoradiation therapy resulted in an area under the receiver operating characteristic curve of 0.88 with 86% sensitivity and 83% specificity for prediction of treatment response.

Conclusions: These results suggest that ADC can be used as a marker for prediction and early detection of response to concurrent chemoradiation therapy in HNSCC.

Head and neck cancer represents ~5% of cancers diagnosed annually in the United States (1) and is more prevalent in developing countries to rank it as the sixth most common cancer in the world (2). These cancers predominately originate from mutations in the mucosal squamous cells and usually present as locoregional disease (3, 4). Treatment of head and neck squamous cell carcinoma (HNSCC) is challenging, as the quality of life of the patient can be severely affected by possible functional losses (impaired swallowing and eating and speech deficit) as well as social losses due to cosmetic deformity from surgery.

Organ-preserving definitive radiation therapy, typically with concurrent chemotherapy, has been accepted as a standard management option for patients with metastatic cervical nodes (1–6). Despite these rigorous treatment methods, the overall survival rate of these patients has not improved significantly as the 5-year survival rate of these patients remains <50% (1, 5, 6). The treatment outcome may be improved by using an optimized treatment strategy tailor-fitted to an individual patient based on imaging biomarkers (7). If the outcome can be predicted before or at an early stage of treatment, the patient could also be spared from ineffective and unnecessary toxicity. Magnetic resonance techniques, including proton spectroscopy (8), diffusion-weighted imaging (DWI; refs. 9–12), and dynamic contrast-enhanced imaging (13), have been proposed as such noninvasive imaging biomarkers for prediction and early detection of response to cancer therapy.

DWI has been suggested as the modality of choice for early detection of treatment response in tumors (9, 10, 14–16). In a recent study, it was reported that in comparison with spin-echo magnetic resonance imaging (MRI) or positron emission tomography (PET), apparent diffusion coefficient (ADC) values resulted in lower false-positives for lesions at the primary site and persistent nodal disease in the postradiation therapy period (17). However, the efficacy of pretreatment ADC values in prediction or for detection of early treatment response (within 1-2 weeks of chemoradiotherapy) in HNSCC has not been reported. Accurate and timely detection of treatment response

Authors' Affiliations: Departments of [1]Radiology, [2]Radiation Oncology, [3]Hematology and Oncology, and [4]Otolaryngology, University of Pennsylvania, Philadelphia, Pennsylvania

Received 5/16/08; revised 10/19/08; accepted 10/21/08.

Grant support: NIH grant RO1-CA102756.

The costs of publication of this article were defrayed in part by the payment of page charges. This article must therefore be hereby marked *advertisement* in accordance with 18 U.S.C. Section 1734 solely to indicate this fact.

Note: Supplementary data for this article are available at Clinical Cancer Research Online (http://clincancerres.aacrjournals.org/).

Requests for reprints: Sungheon Kim, Department of Radiology, New York University, 660 First Avenue, 4th Floor, New York, NY 10016. Phone: 212-263-2717; Fax: 212-263-7541; E-mail: Sungheon.Kim@nyumc.org.

doi:10.1158/1078-0432.CCR-08-1287

Translational Relevance

Organ-preserving definitive radiation therapy, typically with concurrent chemotherapy, without a neck dissection has become an accepted standard management option for locally advanced head and neck squamous cell carcinoma (HNSCC), especially when patients present with metastatic cervical nodes. However, the survival rate of these patients has not improved significantly, raising a question if all patients with locally advanced HNSCC benefit from this treatment paradigm. With the development of organ-preserving surgical techniques, the need to identify radiosensitive HNSCC is even more critical to better triage patients with resectable HNSCC. Apparent diffusion coefficient (ADC) measured by diffusion-weighted magnetic resonance imaging has been proposed as a marker for early response to treatment in brain tumor and breast cancers. However, its efficacy for prediction or detection of early treatment response in HNSCC has not been reported to date. This study was therefore conducted to investigate the efficacy of ADC for prediction and early detection of response to concurrent chemoradiation therapy in locally advanced HNSCC. Our results indicate that ADC can be effectively used as a noninvasive imaging marker for prediction and early detection of response to concurrent chemoradiation therapy in HNSCC.

or presence of nonresponsive tumor can be critical in disease management because the optimal time window for successful surgery or alternative treatment methods may be limited. This study was therefore conducted to investigate the efficacy of ADC in prediction and early detection of treatment response of HNSCC. ADC from the metastatic node was measured three times (before, during, and at the end of chemoradiation therapy).

Materials and Methods

Patient population and treatment. The institutional review board approved this study, and written informed consent was obtained from all 40 subjects before the MRI studies (9 females and 31 males, age 59.8 $\pm$ 10.8 years, recruited between January 2005 and October 2007) who were newly diagnosed with HNSCC with no prior treatment and referred for preoperative chemoradiation therapy. All patients were assessed by a radiation oncologist by clinical reports and a physical examination and had palpable metastatic cervical lymph node masses. Patients received accelerated radiation treatment with 220 cGy/fraction for a total dose of 7,040 cGy to the gross tumor volume in 32 fractions over a total of 44 days, with concurrent chemotherapy (100 mg/m^2 cisplatin on days 1, 22, and 43 of radiation treatment; n = 33) or immunotherapy (400 mg/m^2 cetuximab 3-7 days before radiation therapy and then 250 mg/m^2 cetuximab on days 1, 8, 15, 22, 29, 36, and 43 of radiation treatment; n = 7). Seven patients were excluded from the study because of death unrelated to the treatment (n = 4), claustrophobia (n = 1), withdrawal by patient (n = 1), and severe dental artifacts (n = 1). Hence, analysis of MRI data was done for 33 patients (7 females and 26 males, age 61.0 $\pm$ 10.8 years).

The median follow-up time for the patients was 12 months (range, 6-24 months). Although a post-treatment follow-up of $\geq$6 months may affect the long-term or overall survival, the current study was focused on assessing local control of the metastatic node. Additional therapeutic strategies done after the end of chemoradiation therapy for potential partial responders (PR)/nonresponders including surgery and chemotherapy make it difficult to assess the role of neoadjuvant chemoradiation therapy. Thus, the status at the end of chemoradiation therapy was used as the clinical endpoint in this study. The criterion for a complete responder (CR) was absence of viable tumor on pathology or determination of CR based on clinical/radiologic assessment if surgery was not done. All PR patients were confirmed by the presence of viable tumor on pathology. Individual patient data are shown in Table 1.

All patients underwent three MRI studies, before treatment (Pre-Tx), 1 week after radiation therapy (Wk1-Tx), and $\sim$2 weeks after the completion of the treatment (Post-Tx). Although it was difficult to keep the exact timing of serial MRI scans for all patients, all efforts were made to minimize this variability. The Wk1-Tx scans were conducted at 11.8 $\pm$ 3.7 and 11.4 $\pm$ 2.9 days after initiation of treatment for CR and PR groups with no significant difference (P = 0.81, two-tailed t test with unequal variance). Post-Tx scans were done at 18.0 $\pm$ 8.3 and 10.4 $\pm$ 10.6 days after completion of treatment for CR and PR groups, respectively, also with no significant difference (P = 0.19). The difference in Post-Tx scan time points was mainly due to the large variability in clinical condition of the patient by the end of the treatment. It was assumed that the ADC of the residual nodal masses did not have any substantial change within the range of our Post-Tx scan time points.

Data acquisition. The MRI study was done using a 1.5 T Siemens Sonata scanner (n = 24) or a 3 T Siemens Trio scanner (n = 9; Siemens Medical Systems). A neck array coil or a neurovascular coil was used for 1.5 or 3 T scanners, respectively. T2-weighted (T2w) and T1-weighted (T1w) axial images were acquired using a spin-echo sequence (TR/TE = 4 s/120 ms for T2w and TR/TE = 600/10 ms for T1w). The metastatic nodal masses were identified by a head and neck radiologist on cross-sectional imaging at each MRI scan and were used as primary imaging targets. The metastatic nodes were used instead of the primary tumor because they are less sensitive to artifacts induced by continuous physiologic motion, such as breathing and swallowing, as well as susceptibility artifacts.

Eight axial slices with a field of view of 26 cm and slice thickness of 5 mm were selected to cover the metastatic cervical lymph node for T2 and ADC measurement. Quantitative T2 measurement was done by acquiring a series of T2w images using a spin-echo imaging sequence with four different echo times; 13, 53, 80, and 110 ms (TR = 2 s). DWIs were acquired using a pulsed gradient spin-echo/echo planar imaging sequence (TR/TE = 4 s/89 ms, 4 averages) with three b values: 0, 500, and 1,000 s/mm^2. Huisman et al. have earlier reported that ADC values from the brain are field dependent (18); however, no such studies have been done on the head and neck. Thus, we performed ADC experiments on the neck region of three healthy controls at both 1.5 and 3 T scanners within 1 h and the ADC values from the submandibular glands were compared within each individual from both scanners. For the patient studies, all three scans from each patient were done on the same scanner to reduce any differences due to the magnetic field used. As part of the clinical protocol, contrast-enhanced imaging was done using a single dose of Gd-DTPA (Omniscan; Nycomed) at a concentration of 0.1 mmol/L/kg body weight. The contrast agent was injected at 1 mL/s into an antecubital vein followed by saline flush with a power injector (Medrad). After 10 min, another set of T1w axial images (T1w-Gd) were acquired using a gradient echo sequence (TR/TE = 300/4 ms, flip angle = 90°).

Data analysis. Regions of interest for metastatic nodal mass were drawn by a neuroradiologist (L.L.) based on multislice T1w, T2w, and T1w-Gd images. These regions of interest were used to measure total tumor volume, T2, and ADC values of the node. Because the images of the head and neck region are subject to voluntary as well as involuntary motion, the images were not aligned well with each other in most cases. Thus, before data analysis, all images were coregistered to the spin-echo images with a TE = 80 ms using a two-step nonrigid image registration technique. The first step involved a three-dimensional registration with

affine transformation to minimize global misalignment. Subsequently, each slice was coregistered using a two-dimensional nonrigid registration with second-order discrete sine bases (19) for both X and Y axes. Mutual information (20) was used as the cost function for both coregistration steps. T2 and ADC values were estimated on a pixel-by-pixel basis by fitting a monoexponential function to T2w and diffusion-weighted data, respectively. The median value of the selected region of interest was calculated for each variable. In addition to the volume, T2, and ADC at each time point, change in each variable by Wk1-Tx or Post-Tx was measured by normalizing each variable to the corresponding Pre-Tx value for individual patient. The difference between the two treatment response groups (CR and PR) was assessed using Mann-Whitney U test (21). The receiver operating characteristic analysis (22) was used to evaluate the efficacy of ADC as a predictive marker for response to chemoradiation therapy. Data analysis tools were implemented using IDL routines (ITT Visual Information Solutions).

Results

Response to treatment was determined at the end of chemoradiotherapy based on clinical (n = 11) or pathologic (n = 22) assessment as shown in Table 1. The patients were categorized as CR patients (with no evidence of disease; n = 26) or PR patients (with evidence of residual disease; n = 7). All PR cases were confirmed by pathology for the presence of a viable tumor from the surgically removed nodes. Fifty-seven percent (n = 4) of the PR group presented with metastasis within 6 months after complete dissection of the remaining nodes. In contrast, only 1 patient from the CR group developed distant metastasis and 1 patient exhibited local relapse at the 6-month follow-up (8%, n = 2). This observation indicates that the treatment response assessed at the end of neoadjuvant chemoradiation therapy strongly correlates with the results of 6-month follow-up.

Three healthy volunteers were scanned at both 1.5 and 3 T scanners to test the magnetic field dependency of ADC. Regions of interest were drawn manually on two slices from the left and right submandibular glands. The measured ADC values are provided in Supplementary Table S1. The ADC values measured at 3 T were 4.6 $\pm$ 2.7% higher than those measured at 1.5 T without statistical significance ($P > 0.05$ in all cases). As these results showed a field-independent role of ADC values, we combined the data from patients scanned at the two magnets for group comparisons.

Figure 1 shows representative images from the central section of a metastatic node of a CR patient (primary at base of tongue) at three imaging time points: Pre-Tx (Fig. 1A), Wk1-Tx (Fig. 1B), and Post-Tx (Fig. 1C). The nodal mass (*large arrows*) was

Table 1. Summary of patient information

Patient no.	Sex	Age	Primary site	Tumor staging	Concurrent systemic therapy	Post-Tx surgery	Pathology	6-mo follow-up
1	M	51	Vallecula	$T_2N_{2c}M_0$	Chemo	Y	Positive	DM*
2	M	76	Tonsil	$T_xN_{2b}M_0$	Chemo	Y	Positive	DM
3	M	75	Base of tongue	$T_4N_{2c}M_0$	Chemo	Y	Negative	NED†
4	M	42	Tonsil	$T_2N_{2b}M_0$	Chemo	Y	Negative	NED
5	F	53	Tonsil	$T_xN_{2b}M_0$	Chemo	Y	Negative	NED
6	M	50	Base of tongue	$T_2N_{2a}M_0$	Chemo	Y	Negative	NED
7	M	58	Base of tongue	$T_3N_{2c}M_0$	Chemo	Y	Negative	NED
8	M	76	Larynx	$T_2N_{2b}M_0$	Chemo	Y	Positive	NED
9	M	56	Larynx	$T_2N_3M_0$	Chemo	Y	Positive	DM
10	M	31	Larynx	$T_{4a}N_2M_0$	Chemo	N		NED
11	M	72	Unknown primary	$T_xN_{2b}M_0$	Chemo	N		NED
12	F	78	Unknown primary	$T_{4a}N_2M_0$	Immuno	N		NED
13	F	68	Base of tongue	$T_4N_{2b}M_0$	Chemo	N		DM
14	M	49	Tonsil	$T_3N_{2a}M_0$	Immuno	Y	Negative	NED
15	M	61	Base of tongue	$T_3N_{2a}M_0$	Immuno	Y	Negative	NED
16	M	51	Base of tongue	$T_xN_{2b}M_0$	Chemo	Y	Negative	NED
17	M	64	Unknown primary	$T_xN_3M_0$	Chemo	Y	Positive	DM
18	M	55	Tonsil	$T_3N_{2b}M_0$	Chemo	Y	Negative	NED
19	M	60	Tonsil	$T_4N_1M_0$	Chemo	Y	Positive	NED
20	F	55	Larynx	$T_3N_{2c}M_0$	Chemo	Y	Negative	NED
21	F	62	Tonsil	$T_2N_{2c}M_0$	Chemo	Y	Negative	NED
22	M	65	Unknown primary	$T_xN_{2b}M_0$	Chemo	Y	Negative	NED
23	M	63	Larynx	$T_2N_{2b}M_0$	Chemo	Y	Positive	NED
24	F	48	Tonsil	$T_{4b}N_2M_0$	Immuno	N		Relapse
25	M	72	Base of tongue	$T_4N_{2c}M_0$	Immuno	N		NED
26	F	61	Larynx	$T_xN_{2a}M_0$	Chemo	Y	Negative	NED
27	M	67	Unknown primary	$T_0N_{2b}M_0$	Immuno	N		NED
28	M	52	Base of tongue	$T_1N_{2ab}M_0$	Chemo	Y	Negative	NED
29	M	67	Tonsil	$T_2N_{2b}M_0$	Chemo	N		NED
30	M	70	Tonsil	$T_4N_{1a}M_0$	Chemo	N		NED
31	M	67	Base of tongue	$T_{4a}N_{2c}M_0$	Chemo	N		NED
32	M	59	Base of tongue	$T_4N_{2b}M_0$	Chemo	Y	Negative	NED
33	M	72	Base of tongue	$T_2N_{2b}M_0$	Immuno	N		NED

*DM: distant metastasis.
†NED: no evidence of disease.

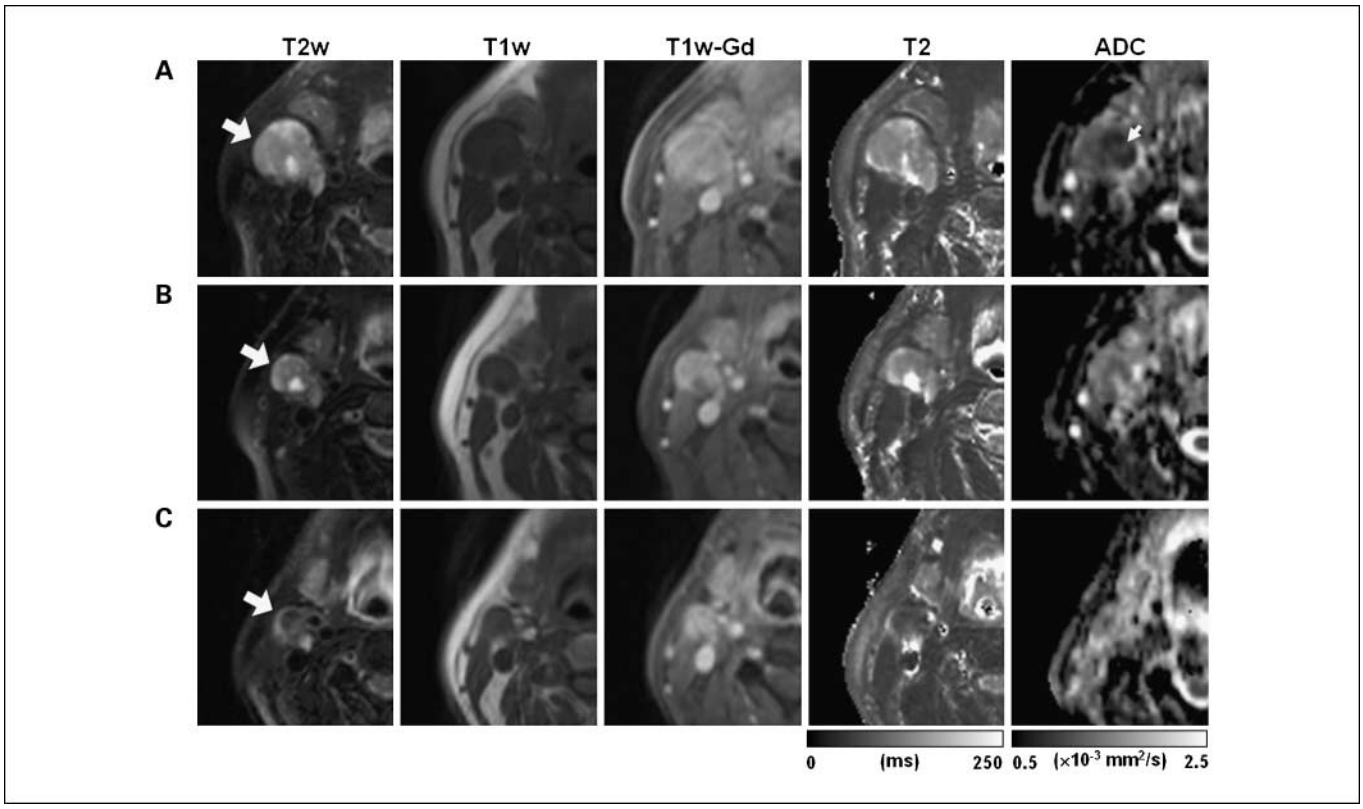

Fig. 1. Representative images of a patient who exhibited CR to treatment as no viable tumor was found at surgery. Images in each row are from three measurement time points: Pre-Tx (*A*), Wk1-Tx (*B*), and Post-Tx (*C*). The T2w, T1w, and T1w-Gd images were windowed to have similar image contrast, whereas T2 and ADC images were scaled based on the grayscale bars shown at the bottom of the corresponding images. *Large arrows,* same nodal metastatic mass that was followed through the treatment course; *small arrow,* central region of the mass with lower ADC values than the peripheral region.

hyperintense on T2w image and hypointense on T1w image and exhibited enhancement on Gd-DTPA-enhanced T1w image. T2 values of the node were 152.6 ± 56.6, 149.7 ± 191.2, and 97.6 ± 26.3 ms for Pre-Tx, Wk1-Tx, and Post-Tx time points, respectively. The central part of the tumor (*small arrow*) had a lower ADC value than the outer region. ADC values of the node were $1.06 \pm 0.28 \times 10^{-3}$, $1.34 \pm 0.28 \times 10^{-3}$, and $1.49 \pm 0.40 \times 10^{-3}$ mm^2/s for Pre-Tx, Wk1-Tx, and Post-Tx, respectively. The residual mass was negative for the presence of viable tumor on histopathology done after surgery. There has been no evidence of a recurrence of disease in this patient as of the writing of this article (17 months after the end of chemoradiation therapy).

Figure 2 shows a case with PR (primary at epiglottic vallecula) in which residual viable tumor was confirmed histopathologically. The node had a similar image contrast on T2w, T1w, and T1w-Gd images as in the case depicted in Fig. 1, indicating the limited sensitivity of these techniques in differentiating the two cases. T2 values were 150.0 ± 30.6, 141.5 ± 57.4, and 109.8 ± 26.1 ms at Pre-Tx, Wk1-Tx, and Post-Tx, respectively. ADC values were $1.22 \pm 0.23 \times 10^{-3}$, $1.47 \pm 0.21 \times 10^{-3}$, and $1.79 \pm 0.26 \times 10^{-3}$ mm^2/s at Pre-Tx, Wk1-Tx, and Post-Tx, respectively. In contrast to the ADC map of the first case shown in Fig. 1, the central part of the mass (*small arrow*) has higher ADC values than the outer region. This patient died with disease (metastasis to lung) 9 months after the completion of the chemoradiation therapy.

A summary of data from all patients is shown by the box-whisker plots in Fig. 3 as a comparison between CR and PR groups in terms of tumor volume and ADC values. For some patients, the tumor shrank dramatically during the treatment such that it was not possible to reliably draw a region of interest to measure any MRI variable. Thus, as indicated in the figure caption, the number of available patient data became smaller at Wk1-Tx and Post-Tx compared with Pre-Tx. In addition to ADC, the nodal volumes of the CR and PR groups were compared at three time points to evaluate the efficacy of nodal volume as a predictive marker for treatment response. Figure 3A indicates that the median nodal volume of the PR group is higher than those of the CR group. However, no significant differences were found between CR and PR groups at any time point ($P > 0.05$). The median volumes decreased significantly in the CR group at Wk1-Tx and Post-Tx ($P < 0.01$) compared with the volumes measured Pre-Tx. To assess the treatment effect on each patient individually, post-treatment data (Wk1-Tx and Post-Tx) were normalized to the respective pretreatment values. There was no significant difference in the normalized nodal volumes between CR and PR groups (Fig. 3B). Figure 3C shows that there was a significant difference ($P < 0.05$) between median ADC values of CR patients ($1.04 \pm 0.19 \times 10^{-3}$ mm^2/s) and PR patients ($1.35 \pm 0.30 \times 10^{-3}$ mm^2/s) at Pre-Tx time point. The median ADC values of CR at Wk1-Tx and Post-Tx were also significantly higher ($P < 0.01$) than the Pre-Tx values, whereas there was no significant change in the median ADC values of PR during

treatment. In terms of the relative change in ADC from each patient, CR patients exhibited a significantly higher ($P < 0.01$ for Wk1-Tx and $P < 0.05$ for Post-Tx) change in ADC than PR (Fig. 3D).

Because T2 values are dependent on the magnetic field strength used, the analysis of T2 values from CR and PR groups was done separately for each magnet (1.5 and 3 T). For comparison, a similar analysis was also done for ADC values. Figure 4 shows a comparison of T2 and ADC values between the CR and PR groups measured at 1.5 T. No significant difference between the CR and PR groups was observed at any time point without (Fig. 4A) or with (Fig. 4B) normalization to Pre-Tx value. For T2 values, a significant difference ($P < 0.01$) was found only in the CR group between Pre-Tx and Post-Tx time points. For the same patient population, the median ADC of the CR group increased significantly ($P < 0.01$) at Wk1-Tx and Post-Tx (Fig. 4C). The normalized Wk1-Tx ADC values were also significantly higher ($P < 0.05$) in CR than in PR (Fig. 4D). These results were similar to the observation when data from both magnets were combined, indicating the field independence of ADC. The CR patients scanned at 3 T also showed similar results; however, because only 1 PR patient was scanned at 3 T, no statistical comparison was attempted between the CR and PR groups.

As shown in Table 1, 7 patients received epidermal growth factor receptor-targeted immunotherapy and they all exhibited CR at the end of therapy. Because only a small number of patients received immunotherapy, it is difficult to assess the prognostic value of diffusion for this particular type of therapy. Within the CR patients, there was no significant ($P > 0.05$) difference in ADC between patients receiving chemotherapy or immunotherapy at all three imaging time points. Within the patients who received conventional chemotherapy, a similar trend was observed in that there was a significant difference in Pre-Tx ADC values between CR and PR patients ($P < 0.05$) and a significant ($P < 0.01$) increase of ADC in CR (Supplementary Fig. S1).

The accuracy of ADC values in differentiating CR from PR patients was tested using binary classification and receiver operating characteristic analyses. The results are summarized in Table 2 with a cutoff value for maximizing the Youden's index (sensitivity + specificity - 1). As shown in Table 2, the best test accuracy was achieved by the normalized ADC value at Wk1-Tx with a sensitivity of 86.4% and specificity of 83.3%.

Discussion

In this study, we investigated the efficacy of ADC for prediction and early detection of treatment response to chemoradiation therapy in HNSCC. The patients who responded favorably to chemoradiation therapy had significantly lower pretreatment ADC than PR patients/nonresponders. In addition, the change in ADC, compared with the pretreatment value, after the first week of chemoradiation therapy, showed the highest test accuracy along with a high sensitivity and specificity of separating CR patients from PR patients. These

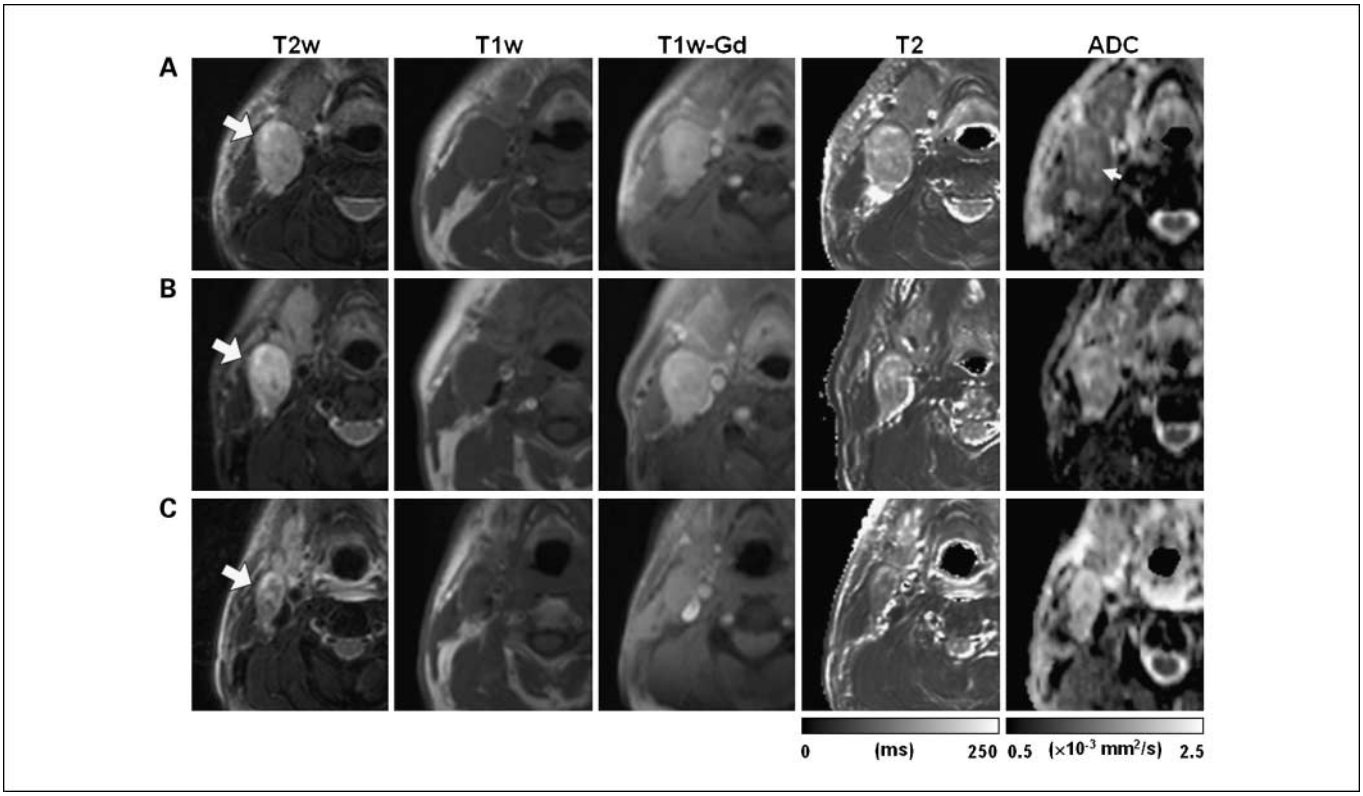

Fig. 2. Representative images of a patient who exhibited PR to treatment as evidenced by the presence of viable tumor at surgery. Images in each row are from three measurement time points: Pre-Tx (*A*), Wk1-Tx (*B*), and Post-Tx (*C*). The T2w, T1w, and T1w-Gd images were windowed to have similar image contrast, whereas T2 and ADC images were scaled based on the grayscale bars shown at the bottom of the corresponding images. *Large arrows,* same metastatic nodal mass that was followed through the treatment course; *small arrow,* central region of the mass with ADC higher than the rim.

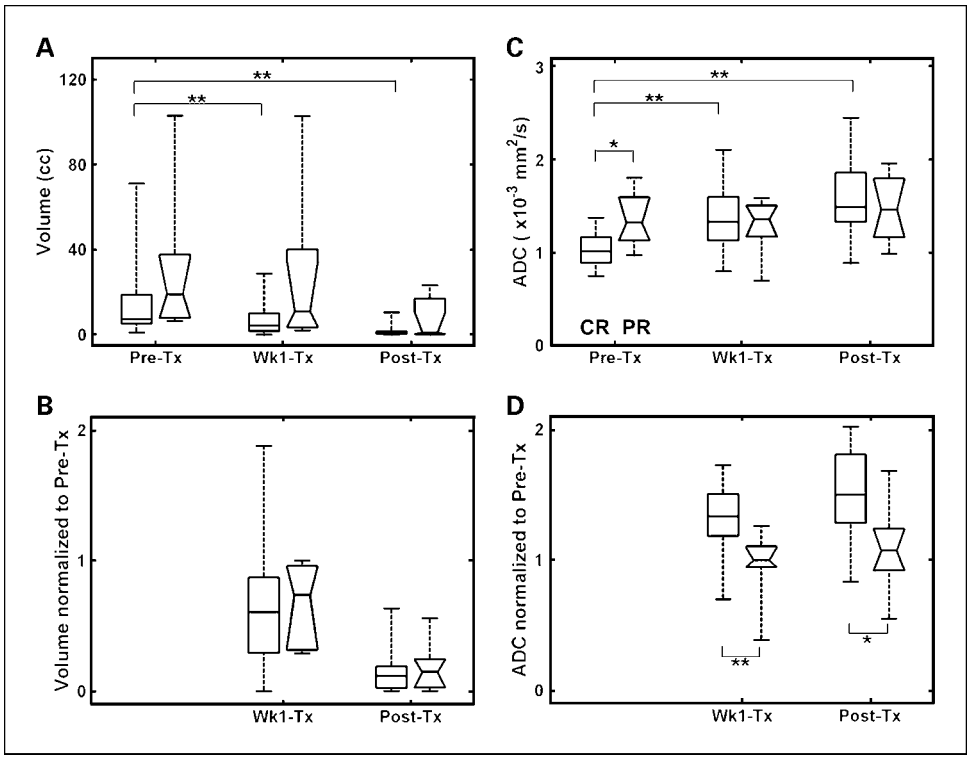

Fig. 3. Comparison of CR (*rectangular boxes*) and PR (*boxes with notches*) groups from all patients scanned using the 1.5 and 3 T scanners in terms of volume (*A*), normalized volume (*B*), ADC (*C*), and normalized ADC (*D*). *Edges,* 25th and 75th percentiles; *middle lines in the boxes,* median values. *Whisker lines,* minimum and maximum values observed. The number of patients for CR group was 26, 22, and 17 for Pre-Tx, Wk1-Tx, and Post-Tx, respectively. The number of patients for PR group was 7, 6, and 5 for Pre-Tx, Wk1-Tx, and Post-Tx, respectively. *, $P < 0.05$; **, $P < 0.01$.

results suggest that ADC can be used as a predictive biomarker for therapeutic response in HNSCC and can thus aid in guiding therapeutic options for patients with HNSCC.

The potential of ADC in diagnosis of head and neck cancers has been reported earlier (23–25). Wang et al. (23) reported that the mean ADC from malignant lesions was significantly smaller than that of benign solid or cystic lesions. It has also been reported that DWI is useful in discriminating metastatic lymph nodes from benign lymphadenopathy or nodal lymphomas (23–25), whereas T1w and T2w images were not specific in differentiating the two pathologies (26). Furthermore, it has been shown that ADC could differentiate radiation

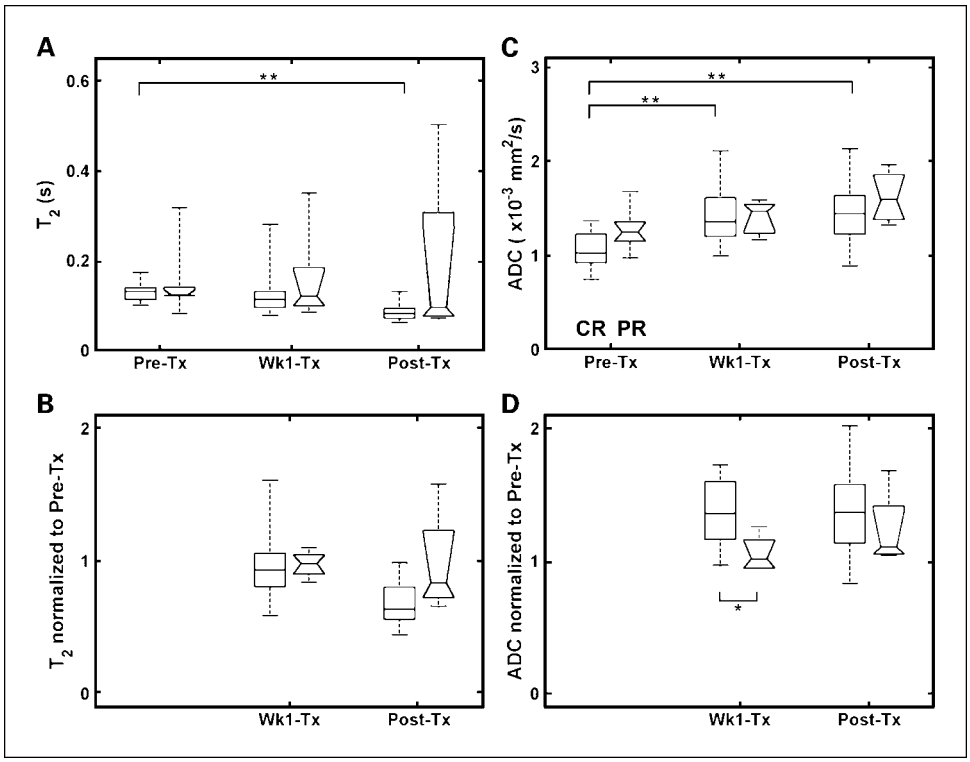

Fig. 4. Comparison of CR (*rectangular boxes*) and PR (*boxes with notches*) groups from the patients scanned using the 1.5 T scanner in terms of T2 (*A*), normalized T2 (*B*), ADC (*C*), and normalized ADC (*D*). *Edges,* 25th and 75th percentiles; *middle lines in the boxes,* median values. *Whisker lines,* minimum and maximum values. The number of patients for CR group was 18, 16, and 12 for Pre-Tx, Wk1-Tx, and Post-Tx, respectively. The number of patients for PR group was 6, 5, and 4 for Pre-Tx, Wk1-Tx, and Post-Tx, respectively. *, $P < 0.05$; **, $P < 0.01$.

response from recurrent tumors (17, 27). In a recent study, it was reported that, in comparison with spin-echo MRI or PET, ADC values resulted in lower false-positives for lesions at the primary site and persistent nodal disease in the postradiation therapy period (17). However, the efficacy of ADC in predicting or detecting treatment response in the head and neck cancer has not been reported earlier.

Preclinical studies in brain tumor models have shown the sensitivity of DWI in detecting early changes induced by chemotherapy (9) or retrovirus-mediated gene therapy (10). Clinical studies on the efficacy of ADC for prediction or early detection of treatment response have been reported for brain tumor (16), breast cancer (12), and cervical cancer (28). As a biomarker for treatment response, Moffat et al. (16) proposed the use of the fractional volume of significantly increased ADC within the tumor after the first 3 weeks of treatment. This method of analysis was termed as functional diffusion mapping. It is important to emphasize that, in comparison with these published studies, we observed a predictive power of ADC even before initiation of treatment and that the sensitivity of early response assessment was highest at 1 week after chemoradiation treatment. Recent studies on a preclinical model of metastatic prostate cancer to the bone (11) and breast cancer (12) also showed significantly increased ADC after 1 week into chemotherapy. Taken together, these studies and our results suggest that the sensitivity of ADC in detecting early therapeutic response depends on the type of cancer, treatment method, and imaging protocol. Nevertheless, the sensitivity of ADC over T2 in detecting response has been reported consistently (10) as observed in this study.

Although the functional diffusion mapping analysis has been used to assess treatment response in brain tumors (16), it is difficult to implement it for organs outside the brain where coregistration of MRIs acquired at different time points may be problematic due to differences in orientation of the images and artifacts induced by cardiac and respiratory motion. Thus, we used the median value of the whole tumor and changes therein during treatment. McVeigh et al. (28) used a similar approach and reported that the pretreatment ADC values (90th percentile) were significantly lower in responders than nonresponders in patients with cervical cancer. This is consistent with our observation as differences between the two groups remained significant when tested with the 75th percentiles instead of the median values (data not shown).

Because ADC values from the extracellular and intracellular spaces are similar in magnitude (29), an increase in ADC after treatment indicates a substantial decrease in restriction of water diffusion within the extracellular space, intercellular space, or both. Gupta et al. (30) reported a lower ADC in malignant brain tumors than benign tumors, which correlated with histologic measures of higher cell density in malignant tumors. Chinnaiyan et al. (31) also reported that a change in ADC was associated with increased number of apoptotic cells and loss of cellularity during apoptosis-induced cancer therapy. Although the mechanism underlying increased water diffusion following cytotoxic chemotherapy in experimental and human tumors is not fully understood, it has been reported that this phenomenon coincides with reduced cell density and enlarged extracellular space due to apoptosis or necrosis (32). Thus, the observed increase in ADC in our study appears to be in line with the expected effect of successful treatment.

Our results with HNSCC are in agreement with a study in cervical cancer (28) in that the pretreatment ADC of CR patients was lower than the PR patients. Because a negative correlation between ADC and cell density has been reported (30), it appears that viable cells in the highly proliferating solid tumor (lower ADC) have a better outcome of response to chemoradiation than tumors that have higher ADC (possibly including areas of necrosis). This may be related to a better perfusion of the actively proliferating solid tumor, which helps delivery of cytotoxic drugs as well as oxygen during radiation therapy. This hypothesis is supported by recent diffusion and perfusion studies (33, 34) in which it was reported that the contrast-enhanced regions of high-grade gliomas have higher blood volume and lower ADC than the low-grade gliomas (33). Recent computed tomography perfusion studies from patients with esophageal squamous cell carcinomas also indicate higher pretreatment blood flow and blood volume in CR patients than PR patients (34, 35).

Current methods for predicting or detecting tumor response include fluorodeoxyglucose PET (36), PET/computed tomography (37), proton (38) or phosphorous (39) magnetic resonance spectroscopy, and dynamic contrast-enhanced MRI (40). Because these methods have been reported on various tumor types using different treatment regimens, it is difficult to make a direct comparison of the results of our study with these methods in terms of its efficacy for prediction and detection of treatment response. However, we believe that the advantage of ADC over PET or dynamic contrast-enhanced MRI is that it does not require injection of an isotope or any contrast agent. The acquisition time for ADC values is ~2 to 3 min, which is much shorter than PET, dynamic contrast-enhanced MRI, or magnetic resonance spectroscopy. In addition to its simplicity in estimating ADC from the DWI data, the ADC value is quantitative and magnetic field independent such that it is

Table 2. Diagnostic characteristic of ADC for differentiating treatment response

Variable	Cutoff value	Sensitivity (%)	Specificity (%)	AUC*
Pre-Tx	1.11×10^{-3} mm^2/s	65 (44, 82)	86 (42, 99)	0.80 (0.62, 0.99)
Wk1-Tx/Pre-Tx	1.11	86 (64, 96)	83 (36, 99)	0.88 (0.74, 1.00)
Post-Tx/Pre-Tx	1.11	82 (56, 95)	80 (30, 99)	0.80 (0.57, 1.00)

NOTE: The cutoff value was selected to maximize the sum of sensitivity and specificity. The numbers in parentheses are the lower and upper limits of 95% confidence interval.
*AUC: area under the receiver operating characteristics curve.

one of the most suitable metrics for multicenter and longitudinal studies.

Although we have shown the potential of ADC in clinical studies of HNSCC, it is challenging to routinely perform DWI in the head and neck due to susceptibility and motion artifacts. We have used a pulsed gradient spin-echo/single-shot echo planar imaging sequence as used in previously reported studies (16, 17, 24). The quality of the DWI data for the head and neck can be improved further by imaging sequences that are less sensitive to susceptibility artifacts, such as line scan DWI (25) or multishot sequence (41), or by using a special anti-susceptibility device on the neck (23). To perform a pixel-wise comparison of imaging variables, images from different sequences (T1, T2, ADC, etc.) need to be coregistered with each other. Image misalignment between different modalities was minimized by using an image coregistration method in this study. However, we feel that this coregistration step could benefit further from improvement in image quality using ways to reduce susceptibility artifacts by methods discussed above as well as methods to account for artifacts induced by voluntary and involuntary motion. This study shows the feasibility of ADC in predicting treatment response of HNSCC using a small cohort of patients recruited between January 2005 and October 2007. In this particular patient population, we had a smaller number of PR patients than CR patients; the effect of this difference on our finding is not known at the present time. Thus, further evaluation of the efficacy of the ADC for clinical application is warranted on a larger patient population.

The current study was done to measure ADC in the metastatic lymph nodes. A similar analysis on tumors at the primary site would be of great interest. However, in comparison with the metastatic node, ADC measurements on the primary site are challenging, as these tumors are generally located in areas prone to artifacts induced by continuous physiologic motion such as breathing and swallowing. In addition, squamous cell carcinomas are located at the air-tissue interface, which increases the susceptibility artifacts on DWIs. Although, in the present study, treatment response of only the metastatic node was assessed, it would be interesting to know whether the ADC values from the metastatic node can also predict overall treatment response. A preliminary assessment of these data can be made from Table 1, which shows the status of each patient at the 6-month follow-up. Although response assessment at the end of treatment was used as an endpoint in the present study, it is interesting to note that, for most patients, the disease status remained unchanged at 6-month follow-up. Future studies would be required to assess the utility of ADC in predicting overall survival or long-term disease-free survival.

There is emerging evidence suggesting that squamous cell carcinomas may have biological differences due to differences in smoking and alcohol use as well as due to molecular alterations, such as epidermal growth factor receptor expression and human papillomavirus infection (1, 2). Due to the small sample size, the present study was not done to address the role of ADC in separating these biological subtypes. However, it is interesting to note that, despite these potential biological differences, our results show that ADC was sensitive in differentiating CR patients from PR patients/nonresponders, indicating the robustness of diffusion imaging as a potential biomarker for prediction and early detection of treatment response.

It is currently difficult to predict which combination of treatment modalities will be best suited for any particular individual. Methods of assessing response to chemoradiotherapy would be useful, as it would permit the oncologist to change therapies, in either type or degree, in cases when the subject does not respond to the initial therapy regimen. Development of noninvasive imaging biomarkers, such as ADC, will aid in accurately predicting and/or assessing treatment response and help in increasing the chance of successful treatment.

Disclosure of Potential Conflicts of Interest

No potential conflicts of interest were disclosed.

References

1. American Cancer Society. Cancer facts & figures 2007. Atlanta: American Cancer Society; 2007.
2. Nagpal JK, Das BR. Oral cancer: reviewing the present understanding of its molecular mechanism and exploring the future directions for its effective management. Oral Oncol 2003;39:213–21.
3. El-Deiry M, Funk GF, Nalwa S, et al. Long-term quality of life for surgical and nonsurgical treatment of head and neck cancer. Archiv Otolaryngol Head Neck Surg 2005;131:879–85.
4. Ang KK, Harris J, Garden AS, et al. Concomitant boost radiation plus concurrent cisplatin for advanced head and neck carcinomas: radiation therapy oncology group phase II trial 99-14. J Clin Oncol 2005;23:3008–15.
5. Zorat PL, Paccagnella A, Cavaniglia G, et al. Randomized phase III trial of neoadjuvant chemotherapy in head and neck cancer: 10-year follow-up. J Natl Cancer Inst 2004;96:1714–7.
6. Bonner JA, Harari PM, Giralt J, et al. Radiotherapy plus cetuximab for squamous-cell carcinoma of the head and neck. N Engl J Med 2006;354:567–78.
7. Ludwig JA, Weinstein JN. Biomarkers in cancer staging, prognosis and treatment selection. Nat Rev 2005;5:845–56.
8. Tzika AA. Proton magnetic resonance spectroscopic imaging as a cancer biomarker for pediatric brain tumors [review]. Int J Oncol 2008;32:517–26.
9. Chenevert TL, McKeever PE, Ross BD. Monitoring early response of experimental brain tumors to therapy using diffusion magnetic resonance imaging. Clin Cancer Res 1997;3:1457–66.
10. Poptani H, Puumalainen A-M, Grohn OH, et al. Monitoring thymidine kinase and ganciclovir-induced changes in rat malignant glioma *in vivo* by nuclear magnetic resonance imaging. Cancer Gene Ther 1998;5:101–9.
11. Lee KC, Sud S, Meyer CR, et al. An imaging biomarker of early treatment response in prostate cancer that has metastasized to the bone. Cancer Res 2007;67:3524–8.
12. Lee KC, Moffat BA, Schott AF, et al. Prospective early response imaging biomarker for neoadjuvant breast cancer chemotherapy. Clin Cancer Res 2007;13:443–50.
13. Raatschen HJ, Simon GH, Fu Y, et al. Vascular permeability during antiangiogenesis treatment: MR imaging assay results as biomarker for subsequent tumor growth in rats. Radiology 2008;247:391–9.
14. Galons JP, Altbach MI, Paine-Murrieta GD, Taylor CW, Gillies RJ. Early increases in breast tumor xenograft water mobility in response to paclitaxel therapy detected by non-invasive diffusion magnetic resonance imaging. Neoplasia (NY) 1999;1:113–7.
15. Chenevert TL, Stegman LD, Taylor JM, et al. Diffusion magnetic resonance imaging: an early surrogate marker of therapeutic efficacy in brain tumors. J Natl Cancer Inst 2000;92:2029–36.
16. Moffat BA, Chenevert TL, Lawrence TS, et al. Functional diffusion map: a noninvasive MRI biomarker for early stratification of clinical brain tumor response. Proc Natl Acad Sci U S A 2005;102:5524–9.
17. Vandecaveye V, De Keyzer F, Nuyts S, et al. Detection of head and neck squamous cell carcinoma with diffusion weighted MRI after (chemo)radiotherapy: correlation between radiologic and histopathologic findings. Int J Radiat Oncol Biol Phys 2007;67:960–71.
18. Huisman TA, Loennekerт, Barta G, et al. Quantitative diffusion tensor MR imaging of the brain: field strength related variance of apparent diffusion coefficient (ADC) and fractional anisotropy (FA) scalars. Eur Radiol 2006;16:1651–8.
19. Ashburner J, Friston KJ. Nonlinear spatial normalization using basis functions. Hum Brain Mapp 1999;7:254–66.
20. Maes F, Collignon A, Vandermeulen D, Marchal G, Suetens P. Multimodality image registration by

maximization of mutual information. IEEE Trans Med Imaging 1997;16:187–98.
21. Mann HB, Wihitney DR. On a test of whether one of two random variables is stochastically larger than the other. Ann Math Stat 1947;18:50–60.
22. Obuchowski NA. Receiver operating characteristic curves and their use in radiology. Radiology 2003; 229:3–8.
23. Wang J, Takashima S, Takayama F, et al. Head and neck lesions: characterization with diffusion-weighted echo-planar MR imaging. Radiology 2001;220:621–30.
24. Sumi M, Sakihama N, Sumi T, et al. Discrimination of metastatic cervical lymph nodes with diffusion-weighted MR imaging in patients with head and neck cancer. AJNR Am J Neuroradiol 2003;24:1627–34.
25. Maeda M, Kato H, Sakuma H, Maier SE, Takeda K. Usefulness of the apparent diffusion coefficient in line scan diffusion-weighted imaging for distinguishing between squamous cell carcinomas and malignant lymphomas of the head and neck. AJNR Am J Neuroradiol 2005;26:1186–92.
26. King AD, Yuen EH, Lei KI, Ahuja AT, Van Hasselt A. Non-Hodgkin lymphoma of the larynx: CT and MR imaging findings. AJNR Am J Neuroradiol 2004;25:12–5.
27. Abdel Razek AA, Kandeel AY, Soliman N, et al. Role of diffusion-weighted echo-planar MR imaging in differentiation of residual or recurrent head and neck tumors and posttreatment changes. AJNR Am J Neuroradiol 2007;28:1146–52.
28. McVeigh PZ, Syed AM, Milosevic M, Fyles A, Haider MA. Diffusion-weighted MRI in cervical cancer. Eur Radiol 2008;18:1058–64.
29. Duong TQ, Ackerman JJ, Ying HS, Neil JJ. Evaluation of extra- and intracellular apparent diffusion in normal and globally ischemic rat brain via ^{19}F NMR. Magn Reson Med 1998;40:1–13.
30. Gupta RK, Cloughesy TF, Sinha U, et al. Relationships between choline magnetic resonance spectroscopy, apparent diffusion coefficient and quantitative histopathology in human glioma. J Neurooncology 2000;50:215–26.
31. Chinnaiyan AM, Prasad U, Shankar S, et al. Combined effect of tumor necrosis factor-related apoptosis-inducing ligand and ionizing radiation in breast cancer therapy. Proc Natl Acad Sci U S A 2000;97:1754–9.
32. Kauppinen RA. Monitoring cytotoxic tumour treatment response by diffusion magnetic resonance imaging and proton spectroscopy. NMR Biomed 2002;15: 6–17.
33. Zonari P, Baraldi P, Crisi G. Multimodal MRI in the characterization of glial neoplasms: the combined role of single-voxel MR spectroscopy, diffusion imaging and echo-planar perfusion imaging. Neuroradiology 2007;49:795–803.
34. Hayano K, Okazumi S, Shuto K, et al. Perfusion CT can predict the response to chemoradiation therapy and survival in esophageal squamous cell carcinoma: initial clinical results. Oncol Rep 2007;18:901–8.
35. Zima A, Carlos R, Gandhi D, Case I, Teknos T, Mukherji SK. Can pretreatment CT perfusion predict response of advanced squamous cell carcinoma of the upper aerodigestive tract treated with induction chemotherapy? AJNR Am J Neuroradiol 2007;28: 328–34.
36. Weber WA. Positron emission tomography as an imaging biomarker. J Clin Oncol 2006;24:3282–92.
37. Weber WA, Figlin R. Monitoring cancer treatment with PET/CT: does it make a difference? J Nucl Med 2007;48 Suppl 1:36–44S.
38. Mukherji SK, Schiro S, Castillo M, Kwock L, Muller KE, Blackstock W. Proton MR spectroscopy of squamous cell carcinoma of the extracranial head and neck: *in vitro* and *in vivo* studies. AJNR Am J Neuroradiol 1997;18:1057–72.
39. Shukla-Dave A, Poptani H, Loevner LA, et al. Prediction of treatment response of head and neck cancers with P-31 MR spectroscopy from pretreatment relative phosphomonoester levels. Acad Radiol 2002; 9:688–94.
40. Thukral A, Thomasson DM, Chow CK, et al. Inflammatory breast cancer: dynamic contrast-enhanced MR in patients receiving bevacizumab—initial experience. Radiology 2007;244:727–35.
41. Deng J, Miller FH, Salem R, Omary RA, Larson AC. Multishot diffusion-weighted PROPELLER magnetic resonance imaging of the abdomen. Invest Radiol 2006;41:769–75.